Molecular Pharmacology Fast Forward. Published on December 4, 2008 as doi:10.1124/mol.108.052340
This article has not been copyedited and formatted. The final version may differ from this version.

Molecular Analysis of the Interaction of Anthrax Adenylyl Cyclase Toxin, Edema Factor, with 2'(3')-*O*-(N-(methyl)anthraniloyl)-Substituted Purine and Pyrimidine Nucleotides[†]

Hesham M. Taha, Jennifer Schmidt[1], Martin Göttle, Srividya Suryanarayana, Yuequan Shen, Wei-Jen Tang, Andreas Gille[2], Jens Geduhn, Burkhard König, Stefan Dove and Roland Seifert[3]

Department of Pharmacology and Toxicology, University of Regensburg, Germany (H.M.T., J.S., M.G); Department of Molecular Biosciences, The University of Kansas, Lawrence, KS (S.S.); Ben May Department for Cancer Research, The University of Chicago, Chicago, IL (W.-J.T.); The College of Life Sciences, Nankai University, People's Republic of China (Y.S.); Institute of Organic Chemistry, University of Regensburg, Germany (J.G., B.K.); Department of Pharmacology, University of Heidelberg, Germany (A.G.); Department of Pharmaceutical and Medicinal Chemistry II, University of Regensburg, Germany (S. D.), Department of Pharmacology, Medical School of Hannover, Germany (R. S.)

Molecular Pharmacology Fast Forward. Published on December 4, 2008 as DOI: 10.1124/mol.108.052340
This article has not been copyedited and formatted. The final version may differ from this version.

Running title

Interaction of edema factor with (M)ANT-nucleotides

[1]Corresponding author

Dr. Roland Seifert

Department of Pharmacology,

Medical School of Hannover

Carl-Neuberg-Straße 1

D-30625 Hannover, Germany

Telephone: +49-511-532-2805. Fax: +49-511-532-4081.

E-mail: seifert.roland@mh-hannover.de

Number of text pages: 38

Number of Tables: 3

Number of Figures: 4

Number of References: 36 (must not be greater than 40)

Number of words in Abstract: 249 (must be below 250 words)

Number of words in Introduction: 408 (must be below 750 words)

Number of words in Discussion: 1497 (must be below 1500 words)

Abbreviations

AC, adenylyl cyclase; ANT, anthraniloyl-; CaM, calmodulin; CyaA, *Bordetella pertussis* adenylyl cyclase toxin; ESI, electrospray ionization; FRET, fluorescence resonance energy transfer; HPLC, high pressure liquid chromatography; k, capacity factor; mAC, mammalian membranous adenylyl cyclase; MANT, methylanthraniloyl-; MS, mass spectroscopy; MW, molecular weight; NDP, nucleoside 5´-diphosphate; NTP, nucleoside 5´-triphosphate; PMEApp, {9-[2-(phosphonomethoxy)ethyl]adenine diphosphate}; EF, full-length edema factor adenylyl cyclase toxin; EF3, catalytic domain of edema factor adenylyl cyclase toxin; R_f, retention factor; R_t, retention time; TLC, thin layer chromatography.

Molecular Pharmacology Fast Forward. Published on December 4, 2008 as DOI: 10.1124/mol.108.052340
This article has not been copyedited and formatted. The final version may differ from this version.

Abstract

Bacillus anthracis causes anthrax disease and exerts its deleterious effects by the release of three exotoxins, i.e. lethal factor, protective antigen and edema factor EF), a highly active calmodulin-dependent adenylyl cyclase (AC). However, conventional antibiotic treatment is ineffective against either toxemia or antibiotic-resistant strains. Thus, more effective drugs for anthrax treatment are needed. Previous studies from our laboratory showed that mammalian membranous AC (mAC) exhibits broad specificity for purine and pyrimidine nucleotides (Mou et al., *Mol Pharmacol* **70**: 878 (2006)). Here, we investigated structural requirements for EF inhibition by natural purine and pyrimidine nucleotides and nucleotides modified with N-methylanthraniloyl (MANT)- or anthraniloyl groups at the 2'(3')-*O*-ribosyl position. MANT-CTP was the most potent EF inhibitor (K_i, 100 nM) among 16 compounds studied. MANT-nucleotides inhibited EF competitively. Activation of EF by calmodulin resulted in effective fluorescence resonance energy transfer (FRET) from tryptophan and tyrosine residues located in the vicinity of the catalytic site to MANT-ATP, but FRET to MANT-CTP was only small. Mutagenesis studies revealed that F586 is crucial for FRET to MANT-ATP and MANT-CTP and that the mutations N583Q, K353A and K353R differentially alter the inhibitory potencies of MANT-ATP and MANT-CTP. Docking approaches relying on crystal structures of EF indicate similar binding modes of the MANT nucleotides with subtle differences in the region of the nucleobases. In conclusion, like mAC, EF accommodates both purine and pyrimidine nucleotides. The unique preference of EF for the base cytosine offers an excellent starting point for the development of potent and selective EF inhibitors.

Molecular Pharmacology Fast Forward. Published on December 4, 2008 as DOI: 10.1124/mol.108.052340
This article has not been copyedited and formatted. The final version may differ from this version.

Introduction

The spore-forming bacterium *Bacillus anthracis* exerts its deleterious effects by production of three major exotoxins, i.e. EF, protective antigen, and lethal factor (Jedrzejas, 2002). EF and lethal factor enter host cells *via* a complex with membrane-associated protective antigen, which acts as a pH-dependent protein transporter. Lethal factor, a specific zinc-metalloprotease, inactivates mitogen-activated protein kinase (Hong et al., 2005). EF possesses ~800 amino acid residues and an apparent molecular weight of ~89 kDa and is a CaM-dependent AC (Drum et al., 2002). After entering host cells, EF forms a complex with CaM, a mammalian regulatory protein that mediates many aspects of calcium-regulated signaling (Shen et al., 2002). The binding of CaM induces a major conformational change in the catalytic domain of EF (Drum et al., 2002). This rearrangement renders EF highly efficient at catalyzing the conversion of ATP into cAMP, disrupting intracellular signaling pathways through excessive activation of cAMP-dependent signaling pathways (Shen et al., 2005).

We resolved several crystal structures of nucleotide·EF·CaM complexes and characterized the amino acids that are important for binding of the substrate ATP and catalysis (Drum et al., 2002; Shen et al., 2002, 2005). Additionally, we showed that mAC and bacterial AC toxins are potently inhibited by MANT-substituted nucleoside 5'-triphosphates (Gille et al., 2004; Mou et al., 2005, 2006; Göttle et al., 2007). MANT-nucleotides are fluorescent, and we exploited this property to suggest conformational changes associated with activation in purified catalytic subunits of mAC (Mou et al., 2005, 2006) and the *Bordetella pertussis* AC toxin, CyaA (Göttle et al., 2007). In addition, by combining crystallographic and molecular modeling approaches, we developed a three-site pharmacophore model for mAC and CyaA, with binding domains for the base, the MANT-group and the polyphosphate chain (Gille et al., 2005; Mou et al., 2006; Wang et al., 2007; Göttle et al., 2007). Those

Molecular Pharmacology Fast Forward. Published on December 4, 2008 as DOI: 10.1124/mol.108.052340
This article has not been copyedited and formatted. The final version may differ from this version.

studies revealed that the catalytic sites of mAC and CyaA exhibit substantial conformational flexibility, accommodating both purine and pyrimidine nucleotides. Despite this flexibility, the structure/activity relationships of MANT-nucleotides at mAC and CyaA are quite different, offering the opportunity to design potent and isoform-selective AC inhibitors.

In contrast to mAC (Gille et al., 2004, 2005; Mou et al., 2005, 2006) and CyaA (Göttle et al., 2007), a detailed analysis of MANT-nucleotide/EF interactions has not yet been presented. Therefore, in the present study, we systematically examined the interactions of natural purine and pyrimidine nucleotides and several (M)ANT-substituted analogues with EF in terms of catalysis, fluorescence changes and molecular modeling.

Materials and Methods

Materials. MANT-GTP, ANT-GTP, MANT-ATP and MANT-ADP were purchased from Jena Bioscience, Germany. PMEApp was supplied by Gilead Sciences, Foster City, CA. GTP, UTP and CTP were purchased from Roche, Mannheim, Germany. ITP, ampicillin, kanamycin, lysozyme enzyme, β-mercaptoethanol, Mes buffer (low moisture content) and dithiothreitol (for molecular biology) were purchased from Sigma-Aldrich, Steinheim, Germany. Tryptone and yeast were purchased from BD Biosciences (Franklin Lakes, NJ). [α–^{32}P]ATP (800 Ci/mmol) was purchased from PerkinElmer, Rodgau Jügesheim, Germany. Aluminum oxide 90 active, (neutral, activity 1, particle size 0.06 - 0.2 mm) was purchased from Biomedicals (Eschwege, Germany). Bovine serum albumin (fraction V, highest quality) was bought from Sigma-Aldrich, Steinheim, Germany. Imidazole

Molecular Pharmacology Fast Forward. Published on December 4, 2008 as DOI: 10.1124/mol.108.052340
This article has not been copyedited and formatted. The final version may differ from this version.

(highest quality), $CaCl_2$, $MnCl_2$ tetrahydrate and $MgCl_2$ hexahydrate (highest quality) were purchased from Merck. For all experiments double-distilled water was used.

(M)ANT-nucleotide synthesis - general procedure. MANT-CTP, MANT-CDP, MANT-UTP, MANT-UDP, MANT-ITP, MANT-IDP, ANT-ATP and ANT-ADP were synthesized according to Hiratsuka (1983) with modifications. The nucleotide (0.33 mmol, 1 eq) was propounded in a small two-neck round flask and dissolved in a minimum amount of water (3 ml). Under continuous stirring a crystalline preparation of (methyl)isatoic anhydride (0.5 mmol, 1.5 eq) was added. After heating to 38°C the pH-value was adjusted to 8.6 and maintained by titration of 1 N NaOH solution for 2 hours. The reaction mixture was extracted three times with chloroform (3 x 20 ml; only for MANT-nucleotides, not for ANT-nucleotides). The aqueous phase was dry-frozen. The received foam showed white to brown color and was applied to a Sephadex® LH-20 column (85 x 2 cm) and subsequently eluted with double-distilled water. The desired product could be detected directly by its blue fluorescence in the collection tubes at λ_{ex} of 366 nm and by TLC. For further purification, reversed-phase preparative HPLC was used to separate (M)ANT-NTP from (M)ANT-NDP. After final dry-freezing white solid compounds (purity >99%) were obtained.

HPLC analysis of (M)ANT-nucleotides. The samples were filtered using a PTFE filter (Chromafil, O-20/15, organic, pore size 0.2 mm; Machery-Nagel, Düren, Germany). A 10 µl sample was analyzed using a HPLC model 1100 (Agilent Technologies, Waldbronn, Germany) fitted with a C18 analytical column (Phenomenex Luna, particle size 3 µm, 150 x 4.60 mm, Aschaffenburg, Germany) and DAD. Data were analyzed using a HPLC-3D ChemStation Rev. A.10.01 [1635]. Gradient elution was performed with 0.05 M ammonium acetate (solvent A) and

Molecular Pharmacology Fast Forward. Published on December 4, 2008 as DOI: 10.1124/mol.108.052340
This article has not been copyedited and formatted. The final version may differ from this version.

acetonitrile (solvent B) at a constant flow rate of 1.0 ml/min. A gradient profile with the following proportions of solvent B was applied [t (min), % B]: [0, 5], [10, 5], [30, 45]. [40, 80]. The chromatograms were monitored at UV absorption at 220 and 254 nm. In addition, a fluorescence detector was used for the analysis of the fluorescent anthraniloylic compounds at λ_{ex} of 350 nm and λ_{em} of 450 nm.

LC/MS online coupling. All samples were filtered using a PTFE filter and injected into a HPLC model 1100 (Agilent Technologies, Waldbronn, Germany). The compound to be analyzed was separated by a C18 column (Phenomenex luna, particle size 3 µm, 150 x 2 mm, Aschaffenburg, Germany). A binary eluent mixture consisting of water (10 mM ammonium acetate) (eluent A) and acetonitrile (eluent B) was pumped with a constant flow of 0.3 ml/min. The following gradient profile was used (t [min], % B): [0, 5], [10, 5], [30, 45]. [40, 80]. The injected volume was 3 µl. Using a triple stage mass spectrometer (TSQ 7000, Thermoquest Finnigan, Toronto, Canada) the mass of the respective compound was determined.

Preparative HPLC. Compound mixtures were dissolved in water (concentration: 30-50 mg/ml) and filtered using a PTFE filter. Compounds were separated using a HPLC model 1100 (Agilent Technologies, Waldbronn, Germany) fitted with a C18 preparative column (Phenomenex Luna, particle size 10 µm, 250 x 21.2 mm). Gradient elution was performed with 0.05 M ammonium acetate (solvent A) and acetonitrile (solvent B) at a constant flow rate of 21 ml/min. The chromatograms were monitored by UV absorption at 220 and 254 nm.

MANT-UTP (*N*-methyl-2'(3')-*O*-anthraniloyl-uridine-5'-triphospate) or [(2R,3S,4R,5R)-5-(2,4-dioxopyrimidin-1-yl)-4(3)-hydroxy-2-[[hydroxy-(hydroxy-

Molecular Pharmacology Fast Forward. Published on December 4, 2008 as DOI: 10.1124/mol.108.052340
This article has not been copyedited and formatted. The final version may differ from this version.

phosphonooxyphosphoryl)oxyphosphoryl]oxymethyl]oxolan-3(4)-yl]2-methylaminobenzoate 182 mg introduced disodium salt of UTP yielded over all purification steps 32 mg (52 μmol, 15%) pure product. R_f = 0.21 (1-propanol:H_2O:NH_3 (32%) = 2:1:1). HPLC (analytic): R_t = 18.78 min, 19.15 min; k = 12.49, 12.75; LC/MS (ESI, H_2O/CH_3CN): m/z = 635.2 [M+NH_4^+] (R_t = 19.69 min, 19.88 min, 100 %), 652.2 [M-H+2NH_4^+] (R_t = 20.15 min, 100%); (-ESI, H_2O/CH_3CN): m/z = 616.2 [M-H^-] (R_t:19.53 min, 20.01 min, 100 %); HPLC (preparative), gradient (t [min], % B: [0, 14], [20, 14], [30, 80]): R_t = 6.07 min, 6.79 min; empirical formula: $C_{17}H_{22}N_3O_{16}P_3$; MW = 617.29.

MANT-UDP (*N*-methyl-2'(3')-*O*-anthraniloyl-uridine-5'-diphospate) or [(2R,3S,4R,5R)-5-(2,4-dioxopyrimidin-1-yl)-4(3)-hydroxy-2-[(hydroxy-phosphonooxyphosphoryl)oxymethyl]oxolan-3(4)-yl]2-methylaminobenzoate. 182 mg introduced disodium salt of UDP yielded over all purification steps 8 mg (15 μmol, 3.8%) pure product. R_f = 0.25 (1-propanol:H_2O:NH_3 (32 %) = 2:1:1). HPLC (analytic): R_t = 19.75 min, 19.93 min; k = 13.19, 13.32; LC/MS (ESI, H_2O/CH_3CN): m/z = 555.2 [M+NH_4^+] (R_t = 20.64 min, 20.94 min, 100%), 572.2 [M-H+2NH_4^+] (R_t = 20.64 min, 20.94 min, 40 %); (-ESI, H_2O/CH_3CN): m/z = 536.2 [M-H^-] (R_t: 20.50 min, 20.78 min, 100%); HPLC (preparative), gradient (t [min], % B: [0, 14], [20, 14], [30, 80]): R_t = 8.79 min, 9.49 min; empirical formula: $C_{17}H_{21}N_3O_{13}P_2$; MW = 537.31.

MANT-CTP (*N*-methyl-2'(3')-*O*-anthraniloyl-cytosine-5'-triphospate) or [(2R,3S,4R,5R)-5-(4-amino-2-oxopyrimidin-1-yl)-4(3)-hydroxy-2-[[hydroxy-(hydroxy-phosphonooxyphosphoryl)oxyphosphoryl]oxymethyl]oxolan-3(4)-yl]2-methylaminobenzoate. 200 mg introduced trisodium salt of CTP yielded over all purification steps 30 mg (48 μmol, 14%) pure product. R_f = 0.24 (1-

Molecular Pharmacology Fast Forward. Published on December 4, 2008 as DOI: 10.1124/mol.108.052340
This article has not been copyedited and formatted. The final version may differ from this version.

propanol:H_2O:NH_3 (32%) = 2:1:1). HPLC (analytic): R_t = 16.86 min, 17.60 min; k = 11.17, 11.70; LC/MS (ESI, H_2O/CH_3CN): m/z = 634.2 [M+NH_4^+] (R_t = 12.98 min, 16.98 min, 100%); (-ESI, H_2O/CH_3CN): m/z = 615.2[M-H^-] (R_t:13.75 min, 17.24 min, 100%); HPLC (preparative), gradient (t [min], % B: [0, 14], [20, 14], [30, 80]): R_t = 4.08 min, 4.61 min; empirical formula: $C_{17}H_{23}N_4O_{15}P_3$; MW = 616.30.

MANT-CDP(*N*-methyl-2'(3')-*O*-anthraniloyl-cytosine-5'-diphospate) or [(2R,3S,4R,5R)-5-(4-amino-2-oxopyrimidin-1-yl)-4(3)-hydroxy-2-[(hydroxy-phosphonooxyphosphoryl)oxymethyl]oxolan-3(4)-yl]2-methylaminobenzoate . 200 mg introduced disodium salt of CDP yielded over all purification steps 2 mg (3.7 µmol, 1%) pure product. R_f = 0.28 (1-propanol:H_2O:NH_3 (32%) = 2:1:1). HPLC (analytic): R_t =18.38 min; k = 12.27; LC/MS (ESI, H_2O/CH_3CN): m/z = 554.2 [M+NH_4^+] (R_t = 18.55 min, 100%); (-ESI, H_2O/CH_3CN): m/z = 535.2 [M-H^-] (R_t:18.66 min, 100%); HPLC (preparative), gradient (t [min], % B: [0, 14], [20, 14], [30, 80]): R_t = 5.80 min; empirical formula: $C_{17}H_{22}N_4O_{12}P_2$; MW = 536.32.

MANT-ITP (*N*-methyl-2'(3')-*O*-anthraniloyl-inosine-5'-triphospate) or [(2R,3S,4R,5R)-5-(6-oxo-1H-purin-9-yl)-4(3)-hydroxy-2-[[hydroxy-(hydroxy-phosphonooxyphosphoryl)oxyphosphoryl]oxymethyl]oxolan-3(4)-yl]2-methylaminobenzoate. 189 mg introduced trisodium salt of ITP yielded over all purification steps 39 mg (61 µmol, 18%) pure product. R_f = 0.31 (1-propanol:H_2O:NH_3 (32%) = 2:1:1). HPLC (analytic): R_t = 19.74 min, 19.86 min; k = 12.65, 12.73; LC/MS (ESI, H_2O/CH_3CN): m/z = 676.2 [M-H+2NH_4^+] (R_t = 20.92 min, 100 %), 659.2 [M+NH_4^+] (R_t = 20.92 min, 80%); (-ESI, H_2O/CH_3CN): m/z = 640.2 [M-H^-] (R_t:20.92 min, 100%); HPLC (preparative), gradient (t [min], % B: [0, 14], [20, 14], [30, 80]): R_t = 8.03 min, 8.23 min; empirical formula: $C_{18}H_{22}N_5O_{15}P_3$; MW = 641.31.

Molecular Pharmacology Fast Forward. Published on December 4, 2008 as DOI: 10.1124/mol.108.052340
This article has not been copyedited and formatted. The final version may differ from this version.

MANT-IDP (*N*-methyl-2'(3')-*O*-anthraniloyl-inosine-5'-diphospate) or [(2R,3S,4R,5R)-5-(6-oxo-1H-purin-9-yl)-4(3)-hydroxy-2-[(hydroxy-phosphonooxyphosphoryl)oxymethyl]oxolan-3(4)-yl]2-methylaminobenzoate. 189 mg introduced disodium salt of IDP yielded over all purification steps 15 mg (27 μmol, 7%) pure product. R_f = 0.35 (1-propanol:H_2O:NH_3 (32%) = 2:1:1). HPLC (analytic): R_t = 20.34 min, 20.58 min; k = 13.07, 13.23; LC/MS (ESI, H_2O/CH_3CN): m/z = 596.3 [M-H+2NH_4^+] (R_t = 21.38 min, 100%), 579.3 [M+NH_4^+] (R_t = 21.38 min, 70%); (-ESI, H_2O/CH_3CN): m/z = 560.2[M-H^-] (R_t: 21.39 min, 21.55 min, 100%); HPLC (preparative), gradient (t [min], % B: [0, 14], [20, 14], [30, 80]): R_t = 10.62 min, 11.36 min; empirical formula: $C_{18}H_{21}N_5O_{12}P_2$; MW = 561.33.

ANT-ATP (2'(3')-*O*-anthraniloyl-adenosine-5'-triphospate) or [(2R,3S,4R,5R)-5-(6-aminopurin-9-yl)-4(3)-hydroxy-2-[[hydroxy-(hydroxy-phosphonooxyphosphoryl)oxyphosphoryl]oxymethyl]oxolan-3(4)-yl]2-aminobenzoate. 189 mg introduced disodium salt of ATP yielded over all purification steps 59 mg (94 μmol, 26%) pure product. R_f = 0.24 (1-propanol:H_2O:NH_3 (32%) = 2:1:1). HPLC (analytic): R_t = 17.44 min; k = 10.07; LC/MS (ESI, H_2O/CH_3CN): m/z = 661.3 [M-H+2NH_4^+] (R_t = 18.12 min, 18.32 min, 100%), 644.2 [M+NH_4^+] (R_t = 18.12 min, 18.32 min, 80%); (-ESI, H_2O/CH_3CN): m/z = 625.2 [M-H^-] (R_t = 18.12 min, 18.33 min, 100%); HPLC (preparative), gradient (t [min], % B: [0, 11], [9, 11], [19, 80]): R_t = 7.07 min, 7.51 min; empirical formula: $C_{17}H_{21}N_6O_{14}P_3$; MW = 626.30.

ANT-ADP (2'(3')-*O*-anthraniloyl-adenosine-5'-diphospate) or [(2R,3S,4R,5R)-5-(6-aminopurin-9-yl)-4(3)-hydroxy-2-[(hydroxy-phosphonooxyphosphoryl)oxymethyl]oxolan-3(4)-yl]2-aminobenzoate. 200 mg

Molecular Pharmacology Fast Forward. Published on December 4, 2008 as DOI: 10.1124/mol.108.052340
This article has not been copyedited and formatted. The final version may differ from this version.

introduced disodium salt of ADP yielded over all purification steps 8 mg (15 µmol, 4%) pure product. R_f = 0.27 (1-propanol:H_2O:NH_3 (32%) = 2:1:1). HPLC (analytic): R_t = 18.09 min; k = 10.73; LC/MS (ESI, H_2O/CH_3CN): m/z = 564.3 [$M+NH_4^+$] (R_t = 18.81 min, 19.04 min, 100%); (-ESI, H_2O/CH_3CN): m/z = 545.2 [$M-H^-$] (R_t = 18.81 min, 19.04 min, 100%); HPLC (preparative), gradient (t [min], % B: [0, 11], [9, 11], [19, 80]): R_t = 8.99 min; empirical formula: $C_{17}H_{20}N_6O_{11}P_2$; MW = 546.32.

Expression and purification of EF and EF3(F586A). The plasmids pProExH6-EF and pProExH6-EF3F586A were prepared as described and amplified in *E. coli* BL21 (DE3)/pUBS520 cells (Drum et al., 2002; Shen et al., 2002, 2005; Guo et al., 2004). The EF3 mutants (H577A, N583A, N583Q, N583H, K353A and K353R) were purified as described (Drum et al., 2002; Shen et al., 2002, 2005; Guo et al., 2004).

Expression and purification of EF was essentially performed as described (Shen et al., 2002) with minor modifications. Specifically, the imidazole concentration in the elution buffer for the HisTrap fast flow rate Ni column was increased to 200 mM. Moreover, imidazole (20 mM) was added into the sample, thus yielding the same imidazole concentration as in the second wash buffer of the Ni column. The following columns were used for EF protein purification; HisTrap fast flow rate affinity Ni column (5 ml) and resource Q (quaternary ammonium salt) strong anionic exchange column (6 ml) (GE Healthcare, Freiburg/Brsg., Germany). EF3(F586A) mutant was expressed and purified essentially as described (Shen et al., 2002) with minor modifications. Specifically, the imidazole concentration in the elution buffer for the Ni column was 200 mM, and imidazole (20 mM) was included in the sample. The HisTrap fast flow rate affinity Ni column (5 ml) was used for immobilized matrix affinity chromatography and the HiPrep 16/10 SP XL column (GE Healthcare) was

Molecular Pharmacology Fast Forward. Published on December 4, 2008 as DOI: 10.1124/mol.108.052340
This article has not been copyedited and formatted. The final version may differ from this version.

used in cation exchange chromatography. CaM was extracted and purified from bovine brain as described (Gopalakrishna and Anderson, 1982). The HiPrep 16/10phenyl FF (high sub) column (GE Healthcare) was used in hydrophobic chromatography purification of CaM.

AC activity assay. For the determination of the potency of AC toxin inhibitors, assay tubes contained 10 μl of MANT-nucleotides at final concentrations from 10 nM to 100 μM as appropriate to obtain saturated inhibition curves and 20 μl of EF, EF3 or EF3(F586A) (10 pM final concentration) in 75 mM Tris/HCl, pH 7.4, containing 0.1% (m/v) bovine serum albumin. Tubes were preincubated for 2 min at 25°C, and reactions were initiated by the addition of 20 μL of reaction mixture consisting of the following components to yield the given final concentrations; 100 mM KCl, 100 μM free Ca^{2+}, 5 mM free Mn^{2+} or Mg^{2+}, 100 μM EGTA, 100 μM cAMP, 100 nM CaM. ATP was added as non-labeled substrate at a final concentration of 40 μM and as radioactive tracer [α–^{32}P]ATP (0.2 μCi/tube). For the determination of K_m and V_{max} values, 10 μM to 1 mM ATP/Mn^{2+} or ATP/Mg^{2+} were added, plus 5 mM of free Mn^{2+} or Mg^{2+}, respectively. Tubes were incubated for 10 min at 25°C, and reactions were stopped by the addition of 20 μL of 2.2 N HCl. Denaturated protein was sedimented by a 1-min centrifugation at 13,000 x g. [^{32}P]cAMP was separated from [α–^{32}P]ATP by transferring the samples to columns containing 1.4 g of neutral alumina. [^{32}P]cAMP was eluted by the addition of 4 ml of 0.1 M ammonium acetate solution, pH 7.0. Blank values were about 0.02% of the total amount of [α–^{32}P]ATP added; substrate turnover was < 3% of the total amount of [α–^{32}P]ATP added. Samples collected in scintillation vials were filled up with 10 ml of double-distilled water and Čerenkov radiation was measured in a PerkinElmer Tricarb 2800TR liquid scintillation

Molecular Pharmacology Fast Forward. Published on December 4, 2008 as DOI: 10.1124/mol.108.052340
This article has not been copyedited and formatted. The final version may differ from this version.

counter. Free concentrations of divalent cations were calculated with WinMaxC (http://www.stanford.edu/~cpatton/maxc.html). V_{max} and K_m values reported in Table 1 and K_i values reported in Tables 2 and 3 were calculated using the Prism 4.02 software (Graphpad, San Diego, CA).

For determination of the potency of AC toxin inhibitors at various EF3 mutants (H577A, N583A, N583Q, N583H, K353A and K353R), the experiments were essentially performed as described for EF and EF3 with some modifications. Specifically, the final enzyme concentrations were increased up to 2 nM in order to account for the lower catalytic activity of the mutants. Moreover, the reaction time was prolonged to 20 min at 30°C. For the determination of V_{max} and K_m, the ATP/Mn^{2+} concentration ranged from 100 μM to 4 mM. The higher substrate concentrations compared to EF were essential in order to obtain saturated enzyme kinetics.

For determination of the potency of AC toxin inhibitors at EF3 in absence of both CaM and Ca^{2+}, experiments were performed as described for standard experiments with some modifications in order to increase assay sensitivity. Specifically, the final enzyme concentration was increased up to 5 nM, and the reaction was stopped after 30 min incubation at 30°C. Moreover, in competition experiments, the concentration of unlabeled ATP was decreased to 20 μM and [α–^{32}P]ATP was used at a high amount (1.0 μCi/tube). For the determination of V_{max} and K_m, the same modifications were performed, except that the ATP/Mn^{2+} concentration was varied.

For studying of the inhibition mechanism of the EF3 by MANT-nucleotides, enzyme saturation experiments were performed in the presence of various inhibitor concentrations (Fig. 1). Assay tubes contained MANT-nucleotides at final concentrations from 0.5 μM to 20 μM as appropriate according to the potency of the

Molecular Pharmacology Fast Forward. Published on December 4, 2008 as DOI: 10.1124/mol.108.052340
This article has not been copyedited and formatted. The final version may differ from this version.

inhibitor. For the basal saturation curve double-distilled water was added instead of the inhibitor. Assay tubes contained 50 µM to 600 µM ATP/Mn^{2+}, 10 pM EF3 in 75 mM Tris/HCl, pH 7.4 and 0.1% (m/v) bovine serum albumin. Tubes were preincubated for 2 min at 25°C, and reactions were initiated by the addition of 20 µl of reaction mixture consisting of the following components to yield the given final concentrations; 100 mM KCl, 100 µM free Ca^{2+}, 5 mM free Mn^{2+}, 100 µM EGTA, 100 µM cAMP, 100 nM CaM, and [α–^{32}P]ATP (0.2 µCi/tube).

Fluorescence resonance energy transfer (FRET) experiments for monitoring inhibitor binding to EF. Fluorescence experiments were performed using quartz UV ultra-microcuvettes from Hellma (Müllheim, Germany, type 105.251-QS, light path length 3 x 3 mm, center 15 mm, total volume 70 µl and type 105.250-QS, light path length 10 x 2 mm, center 15 mm, total volume 150 µl) in a thermostated multicell holder at 25°C in a Varian Cary Eclipse fluorescence spectrometer (Varian, Darmstadt, Germany). In case of 150 µl cuvettes, 140 µl of buffer consisting of 100 mM KCl, 100 µM $CaCl_2$, 10 mM $MnCl_2$ and 25 mM HEPES/NaOH, pH 7.4, was added into the cuvette. Five µl of 10 µM full-length EF (final concentration 300 nM), 5 µl of 10 µM CaM (final concentration 300 nM) and MANT-ATP or MANT-CTP (300 nM each) were added. In case of experiments with 70 µl cuvettes, volumes were adjusted stoichiometrically. The results obtained with 70 µl- and 150 µl-cuvettes were identical, with the 70 µl-cuvettes offering an opportunity to save EF/EF3 mutant protein.

Steady-state fluorescence emission spectra of nucleotides were recorded at low speed in the scan mode from λ_{em} 300 nm to 550 nm with λ_{ex} 280 nm. Fluorescence recordings were analyzed with the spectrum package of the Varian

Molecular Pharmacology Fast Forward. Published on December 4, 2008 as DOI: 10.1124/mol.108.052340
This article has not been copyedited and formatted. The final version may differ from this version.

Cary Eclipse software version 1.1. Baseline fluorescence (buffer alone) and the baseline-corrected nucleotide-dependent emission of each concentration of the ligand (buffer + nucleotide) were subtracted from the spectra shown in Fig. 2. In the competition experiments shown in Fig. 3, MANT-nucleotides were displaced from the EF catalytic site using PMEApp. In some experiments, we also directly excited MANT-nucleotides at λ_{ex} 350 nm and monitored fluorescence emission from 400-500 nm.

Modeling of the nucleotide binding mode to EF-CaM. Docking studies were performed with the molecular modeling package SYBYL 7.3 (Tripos International, St. Louis, MO) on a Silicon Graphics Octane workstation. An initial computer model was generated from the crystal structure of EF-CaM in complex with 2'-deoxy-3'ANT-ATP, PDB 1lvc, chain C (Shen et al., 2002). Yb^{2+} was replaced by Mg^{2+}. Water molecules were added from the crystal structure of EF-CaM in complex with 3'-deoxy-ATP, PDB 1k90 (Drum et al., 2002). Hydrogens were added and AMBER_FF99 charges assigned to the protein and the water. 2'-Deoxy-3'ANT-ATP was provided with Gasteiger-Hueckel-charges. The model was then pre-optimized with the AMBER_FF99 force field (Cornell et al., 1995) (ligand and Mg^{2+} fixed, distant dependent dielectric constant $\varepsilon = 4$, 25 cycles steepest descent, followed by Powell conjugate gradient, end gradient of 0.1 kcal $mole^{-1}$ $Å^{-1}$) were performed.

Initial docking positions of 2'-MANT-CTP, 3'-MANT-CTP and 3'-MANT-ATP were based on the localization and conformation of 2'-deoxy-3'-ANT-ATP in this model, allowing the modification of rotatable bonds. Each complex was refined in a stepwise approach. Firstly, ~25 minimization cycles with fixed ligand (AMBER_FF99 force field, steepest descent, $\varepsilon = 4$), secondly, minimization of the ligand and the surrounding protein residues (distance up to 6 Å) with the Tripos force field (Clark et

Molecular Pharmacology Fast Forward. Published on December 4, 2008 as DOI: 10.1124/mol.108.052340
This article has not been copyedited and formatted. The final version may differ from this version.

al., 1989), (Powell conjugate gradient, ε = 1, end gradient of 0.05 kcal mole^{-1} Å^{-1}), and, thirdly, final refinement with fixed ligand (AMBER_FF99 force field, Powell conjugate gradient, ε = 4, end gradient of 0.01 kcal mole^{-1} Å^{-1}). The RMS deviation between the three minimized models amounts to 0.2 – 0.25 Å if all atoms of the protein are considered.

Results

Kinetic analysis of the catalytic activities of EF, EF3 and various EF3 mutants. In Table 1, the V_{max} and K_m values of EF, EF3 and various EF3 mutants in the presence of Ca^{2+}/CaM and Mn^{2+} are summarized. The difference between EF and EF3 is that EF3 does not contain the binding domain for protective antigen (Drum et al., 2002; Shen et al., 2005). The V_{max} and K_m values were very similar for EF and EF3. In EF3(F586A), V_{max} decreased by about 50% compared to EF3 with little change in K_m. The H577A mutation dramatically reduced V_{max} and moderately decreased K_m. Substitution of N583 with other hydrogen-bond-forming residues such as Q583 or H583 significantly reduced V_{max} together with a 10-50-fold increase in K_m. Mutation of K353 into A353 reduced V_{max} 55-fold and increased K_m 10-fold. EF(K353R) exhibited about 5-fold reduced V_{max} and similar K_m compared to the EF3. There are some differences in the kinetic parameters of EF3 and EF3 mutants in the presence of Mg^{2+} (Drum et al., 2002) and Mn^{2+} (Table 1), supporting the view that these divalent cations interact differentially with ACs (Gille et al., 2004; Mou et al., 2005, 2006; Göttle et al., 2007). Since the FRET signals presented below were much smaller in the presence of Mg^{2+} than Mn^{2+} (data not shown), we decided to conduct all enzymatic studies in the presence of Mn^{2+} as well.

Molecular Pharmacology Fast Forward. Published on December 4, 2008 as DOI: 10.1124/mol.108.052340
This article has not been copyedited and formatted. The final version may differ from this version.

We also determined the kinetic parameters of EF3 in the presence of Mn^{2+} but in the absence of Ca^{2+}/CaM. By removing of both CaM and Ca^{2+} from the reaction mixture, V_{max} was reduced about 2000-fold, but there was no effect on K_m.

Inhibition of the catalytic activity of EF, EF3 and various EF3 mutants by (M)ANT-nucleotides. Table 2 summarizes the K_i values of MANT-ATP and MANT-CTP at EF, EF3 and EF3 mutants in the presence of Mn^{2+}. At EF and EF3, MANT-CTP was a 5-10-fold more potent inhibitor than MANT-ATP. The F586A mutation reduced the inhibitory potencies of MANT-ATP and MANT-CTP by 5-6-fold, whereas the H577A mutation did not decrease inhibitor potency. The N583A mutation decreased nucleotide-potency by 90-100-fold. The N583Q substitution reduced the potency of MANT-ATP by 70-fold and the potency of MANT-CTP by 2,500-fold. For the N383H mutant, a 200-300-fold decrease in potency of MANT-ATP and MANT-CTP was observed. The K353A substitution reduced the potency of MANT-ATP by less than 20-fold, whereas the potency of MANT-CTP was reduced by more than 500-fold. The K_i value of MANT-ATP at EF3(K353R) increased just 3-fold, while the K_i value of MANT-CTP increased by 65-fold. The omission of Ca^{2+}/CaM had only little effect on the K_i values of both MANT-ATP and MANT-CTP at EF3.

Fig 1 shows the double-reciprocal analysis of EF3 inhibition kinetics by MANT-ATP and MANT-CTP according to Lineweaver-Burk. The linear regression lines intersected at the y-axis, i.e. V_{max} remained constant, whereas K_m increased with increasing inhibitor concentration.

Table 3 summarizes the K_i values of various natural purine and pyrimidine nucleotides and various (M)ANT-NDPs and -NTPs at EF in the presence of Mn^{2+} and Mg^{2+}. In general, inhibitor potencies were higher with Mn^{2+} than with Mg^{2+}, but the impact of the cation varied with the nucleotide studied. For example, ANT-ATP,

Molecular Pharmacology Fast Forward. Published on December 4, 2008 as DOI: 10.1124/mol.108.052340
This article has not been copyedited and formatted. The final version may differ from this version.

MANT-CTP and MANT-CDP were about 10-fold more potent in the presence of Mn^{2+} than in the presence of Mg^{2+}, whereas for MANT-GTP, the affinity difference was less than 2-fold. A differential impact of Mg^{2+} and Mn^{2+} on MANT-nucleotide-affinity was also noted for mAC and CyaA (Gille et al., 2004; Mou et al., 2005, 2006; Göttle et al., 2007)

All natural nucleoside 5'-triphosphates studied inhibited the catalytic activity of EF with CTP being the most potent inhibitor. Substitution of the 2'(3')-*O*-ribosyl group with a (M)ANT group substantially increased inhibitor potency. For example, in the presence of Mn^{2+}, MANT-CTP showed about 60-fold higher potency at EF than the unmodified nucleotide. The potency-increasing effect of the (M)ANT-group depended on the specific nucleotide examined. For example, in the presence of Mn^{2+}, the potency of MANT-GTP was just 3.5-fold higher than the potency of GTP. (M)ANT-NDPs were less potent EF inhibitors than the corresponding (M)ANT-NTPs. In the presence of Mn^{2+}, MANT-ATP and ANT-ATP were similarly potent EF inhibitors, whereas in the presence of Mg^{2+}, MANT-ATP was about 4-fold more potent than ANT-ATP. MANT-GTP was up to 2.5-fold more potent than ANT-GTP.

Analysis of the interaction of MANT-nucleotides with EF3 in FRET experiments. At an excitation wavelength of 280 nm, tryptophan and tyrosine residues in proteins are excited, emitting light at 350 nm (Lakowicz 1999) which can then excite the (M)ANT group of nucleotides (Hiratsuka 1983), provided sufficient proximity between donor and acceptor. Such energy transfer results in increased fluorescence of the MANT-group at 420-450 nm in mAC and CyaA, reflecting the fact that the MANT-group is in a hydrophobic environment (Mou et al., 2005, 2006; Göttle et al., 2007). Previous studies with mAC showed that in the presence of Mn^{2+}, FRET signals were much larger than in the presence of Mg^{2+} (Mou et al., 2005). Preliminary

Molecular Pharmacology Fast Forward. Published on December 4, 2008 as DOI: 10.1124/mol.108.052340
This article has not been copyedited and formatted. The final version may differ from this version.

studies with EF3 showed that the Mn^{2+}-preference also applies to the toxin (data not shown). Therefore, all subsequent FRET studies with EF3 were conducted in the presence of Mn^{2+} (see Materials and Methods).

In the absence of CaM, EF3 exhibits a strong emission peak at 350 nm when excited at 280 nm under steady-state conditions (Figs. 2A and 2C). Upon addition of the EF activator CaM, an additional prominent fluorescence peak with an emission maximum at 440 nm appeared with MANT-ATP (Fig. 2A), reflecting FRET from tryptophan and tyrosine residues to the MANT-group. In EF(F586A), the endogenous tryptophan and tyrosine fluorescence was similar as in EF3, but the FRET signal (difference in fluorescence at an emission wavelength of 440 nm in the presence and absence of calmodulin) was reduced by 55% (Fig. 2B). With MANT-CTP, only a small FRET signal was apparent with EF3 upon addition of CaM (Fig. 2C). Even an increase of the final CaM concentration to 3 μM, yielding a 10-fold molar excess of CaM relative to EF3, did not increase FRET with MANT-CTP (data not shown). The small FRET signal with MANT-CTP was reduced by 43% in EF(F586A) (Fig. 2D). Analysis of the EF mutants H577A, N583A, N583Q, N583H and K353A with MANT-ATP and MANT-CTP revealed no FRET at all (data not shown). With CaM and MANT-nucleotides alone, i.e. in the absence of EF3, no FRET signal was observed (data not shown).

In FRET experiments, the appearance of the new fluorescence peak at λ_{em} 440 nm would have been expected to be accompanied by a decrease in fluorescence at λ_{em} 350 nm as was the case for mAC (Mou et al., 2005, 2006) and CyaA (Göttle et al., 2007). Rather, a small increase in EF3 fluorescence upon CaM addition was observed (Fig. 2). An explanation for these findings could be that the endogenous tyrosine and tryptophan fluorescence of EF3 is quenched by surrounding polar amino acids such as aspartate, glutamate and histidine (Lakowicz,

Molecular Pharmacology Fast Forward. Published on December 4, 2008 as DOI: 10.1124/mol.108.052340
This article has not been copyedited and formatted. The final version may differ from this version.

1999). Upon addition of CaM, a large conformational change occurs in EF3 (Shen et al., 2002; Drum et al., 2002), abrogating the quenching effects of polar amino acids and, thereby, masking the expected decrease in fluorescence at λ_{em} 350 nm.

Control experiments with dimethyl sulfoxide ranging from 0-100% (vol/vol) (Hiratsuka, 1983) revealed that MANT-ATP and MANT-CTP possess similar relative increases in fluorescence upon exposure to a hydrophobic environment (λ_{ex} 350 nm; λ_{em} 400-500 nm) (data not shown). Thus, differences in biophysical properties of nucleotides do not account for the different FRET responses observed with MANT-ATP and MANT-CTP upon interaction with EF. We also studied the interaction of EF with MANT-nucleotides by exciting nucleotides directly at λ_{em} 350 nm. As was true in the FRET experiments (Fig. 2), the response observed with MANT-ATP at λ_{em} 450 nm was greater than with MANT-CTP (data not shown).

Fig. 3 shows the kinetics of FRET experiments with MANT-ATP and MANT-CTP at a fixed emission wavelength of 440 nm. Sequential addition of EF3 and CaM resulted only in small fluorescence increases, reflecting the far end of the tryptophan/tyrosine emission spectrum (see Fig. 2). Addition of MANT-nucleotides to cuvettes instantaneously resulted in substantial fluorescence increases, reflecting FRET. Addition of the high-affinity EF inhibitor and non-fluorescent nucleotide analog PMEApp (1 μM) (Shen et al., 2004) to cuvettes reduced the fluorescence signals with both MANT-nucleotides (300 nM each), but the inhibitory effect of PMEApp was more pronounced and more rapid in onset with MANT-ATP than with MANT-CTP.

Modeling of the binding modes of MANT-nucleotides to EF-CaM. The crystal structure of EF in complex with CaM and 2'-deoxy-3'-ANT-ATP (PDB 1lvc, Shen et al., 2002) served as basis for the docking of MANT-CTP and MANT-ATP.

Molecular Pharmacology Fast Forward. Published on December 4, 2008 as DOI: 10.1124/mol.108.052340
This article has not been copyedited and formatted. The final version may differ from this version.

Fig. 4A shows that the nucleotide binding site of EF is a spacious cavity located at the interface of two structural domains, C_A (D294 – N349, A490 – K622) and C_B (V350 – T489). Three switches, A (Q507 – L549), B (G578 – N591), and C (R630 – T659), which strongly change their conformation and position on the transition from EF alone to EF-CaM (Drum et al., 2002, Shen et al., 2002) cover the catalytic site in the EF-CaM state. A metal cation (Yb^{2+} in the template, replaced by Mg^{2+} in the models) is involved in ionic interactions with D491, D493 and the α-phosphate of the nucleotides. The MANT group is aligned in parallel with the phenyl ring of F586. Thus, hydrophobic interactions account for the generally higher potency of the ANT- and MANT-derivatives compared to their natural parent nucleotides (Table 3).

The docking approaches were performed to suggest possible reasons why MANT-CTP inhibits EF-CaM more potently than MANT-ATP. Figs. 4B and 4D compare the putative binding mode of 3'-MANT-CTP and 3'-MANT-ATP in more detail. The common structures of both molecules interact with EF-CaM in the same manner. In the minimized models, the ribosyl rings adopt a 3'-exo conformation like the ribosyl moiety of 3'-MANT-ATP in complex with mAC (Mou et al., 2006). The triphosphate moieties fit into a deep polar pocket forming ionic interactions with the lysines 346, 353 and 372 as well as an H bond with S354 (γ-phosphate). These interactions account for the higher inhibitory potencies of the triphosphates compared to the diphosphate analogs in Table 3. The ring oxygens of the ribosyl moieties are hydrogen-bonded to the amide NH_2 of N583. The 2'-OH groups approach the side chain of L348. Additionally to the parallel fit to F586, the 3'-MANT substituents interact via their amino function with H351.

The nucleobases show both shared and different interactions. Most striking is the flat alignment with the side chain of N583. In the case of 3'-MANT-CTP, such type of interaction is more favorable since the oxygen in 2'-position of the base may

Molecular Pharmacology Fast Forward. Published on December 4, 2008 as DOI: 10.1124/mol.108.052340
This article has not been copyedited and formatted. The final version may differ from this version.

align with the positive pole of the amide dipole. However, this difference cannot be the only reason for the higher potency compared to MANT-ATP, because also on the N583A mutant, MANT-CTP is more potent than its ATP analog (Table 3). Considering the farther environment of the cytosine oxygen, additional reasons can be suggested. In the minimized model, it is in a 3.3 Å distance from the guanidino group of R329. Moreover, a water molecule can be placed in an ideal position into the EF-MANT-CTP model where it forms three H bonds, bridging the cytosine oxygen with the side chains of R329 and E580. The NH_2 groups of the cytosine and adenine moieties interact similarly with EF-CaM via H bonds to backbone oxygens (3'-MANT-CTP to G578 and/or T579, 3'MANT-ATP to T548 and T579). The signifinace of these interactions is confirmed by the lower potency of MANT-UTP and MANT-GTP (Table 3). Interestingly, the N583H mutant disproportionately reduces the potency of MANT-ATP, whereas on the N583Q species, MANT-CTP is even less potent than its ATP analog. In the former case, an alignment of the heterocycles should be still possible. However, the larger glutamine side chain in N583Q restricts the binding cavity for the nucleobases so that the mode of interaction changes. As suggested for MANT-CTP, also the affinity of the other nucleotides to EF3 and EF mutants may be affected by a specific arrangement of water molecules.

The MANT nucleotides used in the assays are mixtures of 2'-MANT and 3'-MANT isomers, and there is spontaneous isomerization between the two species under physiological conditions (Hiratsuka, 1983, 2003; Jameson and Eccleston, 1997). So far, only the putative binding mode of 3’-MANT-isomers has been considered. The question arises whether the MANT group may fit to the same EF-CaM site in both isomers as shown for the binding of MANT-nucleotides to CyaA (Göttle et al., 2007). Fig. 4C indicates that 2'-MANT-CTP may indeed interact with EF-CaM in a very similar position like its 3'-MANT analog. The main difference is a 3'-

Molecular Pharmacology Fast Forward. Published on December 4, 2008 as DOI: 10.1124/mol.108.052340
This article has not been copyedited and formatted. The final version may differ from this version.

endo conformation of the ribosyl moiety, present also in the complex of 3'-deoxy-ATP with EF-CaM (Drum et al., 2002). This geometry implies an axial position of the 2'-MANT group which may then project to the space between H351 and F586. Additionally, an intramolecular H bond between the 3'-hydroxy group and the proximal α-phosphate oxygen is possible. Fig. 4E, showing the alignment of 2'-MANT-CTP, 3'-MANT-CTP and 3'-MANT-ATP in the docked poses, indicates a close fit of the 2'-MANT and 3'-MANT isomers. Only the positions of the MANT groups themselves are slightly different (variability of the triphosphate conformation is due to the individual minimization courses).

Discussion

The major goal of the present study was to characterize the interaction of the catalytic site of EF with (M)ANT-nucleotides possessing various purine and pyrimidine bases in order to better understand the molecular mechanisms of EF inhibition and to provide the basis for the rational development of potent and selective EF inhibitors. Such EF inhibitors could be useful compounds to treat EF toxinemia and antibiotic-resistant *Bacillus anthracis* strains (Jedrzejas, 2002).

In previous studies, we developed a three-site pharmacophore model for mAC and CyaA toxin with binding regions for the base, the MANT-group and the polyphosphate chain (Gille et al., 2005; Mou et al., 2006; Wang et al., 2007; Göttle et al., 2007). Those studies revealed that the MANT-group and the polyphosphate chain are the major determinants of inhibitor potency, whereas the base plays a relatively small role in this respect. This is reflected by the fact that the catalytic sites of mAC

Molecular Pharmacology Fast Forward. Published on December 4, 2008 as DOI: 10.1124/mol.108.052340
This article has not been copyedited and formatted. The final version may differ from this version.

and CyaA are conformationally flexible and accommodate both purine and pyrimidine nucleotides.

Likewise, in EF, the (M)ANT-group and the length of the polyphosphate chain have a substantial impact on inhibitor potency, and EF accommodates various purine and pyrimidine bases (Table 3). These data indicate that the three-site binding model developed for mAC and CyaA can also be extended to EF. The structure/activity relationships of (MANT)-nucleotides at EF, CyaA and mAC are different, indicating that in principle, the development of potent and AC isoform-specific inhibitors is feasible. Most strikingly, CTP inhibited EF more than 400-fold more potently than mAC (Table 3) (Gille et al., 2005). Substitution of the 2'(3')-*O*-ribosyl position of CTP with a MANT group decreased the K_i value from 5 μM to 100 nM, yielding an EF inhibitor that is even 5-10-fold more potent than MANT-ATP in the presence of Mn^{2+} (Tables 2 and 3).

The highly unexpected preference of EF for the base cytosine prompted us to analyze EF inhibition by MANT-CTP and MANT-ATP in more detail. The analysis of enzyme inhibition kinetics revealed that both MANT-CTP and MANT-ATP are competitive EF inhibitors, i.e. they bind to the same site as, and freely compete with, the substrate ATP (Fig. 1). These data rule out the existence of a hitherto unidentified cytosine base-preferring nucleotide-binding site in the structurally very complex EF protein (Fig. 4A) (Drum et al., 2002; Shen et al., 2002). Kinetic FRET competition experiments with the non-fluorescent ATP analog PMEApp revealed that both MANT-ATP and MANT-CTP reversibly bind to the catalytic site (Fig. 3), corroborating the competitive inhibition mode and the existence of a single nucleotide-binding site in EF. The faster displacement of MANT-ATP from EF by PMEApp compared to the displacement of MANT-CTP is explained by the higher affinity of EF for MANT-CTP.

Molecular Pharmacology Fast Forward. Published on December 4, 2008 as DOI: 10.1124/mol.108.052340
This article has not been copyedited and formatted. The final version may differ from this version.

In order dissect possible differences in the binding modes of MANT-ATP and MANT-CTP to EF, we studied their interaction with several EF mutants in terms of enzyme inhibition and fluorescence spectroscopy. A previous study had shown that F586 mediates π-stacking interactions with 2'-deoxy-3'-ANT-ATP, resulting in a fluorescence increase upon excitation of the ANT-group (Shen et al., 2002). In agreement with those data, mutation of F586 reduced the potency of MANT-ATP and largely reduced the CaM-dependent FRET of MANT-ATP (Table 2 and Fig. 2). F586 is also important for the interaction with MANT-CTP as is revealed by the 6-fold reduction in potency. However, compared to MANT-ATP, the FRET signal with MANT-CTP in EF was much smaller, and the F586A mutation had a smaller inhibitory effect on the FRET. This difference in FRET cannot be explained by a lower CaM-affinity of EF bound to MANT-CTP compared to the protein complex bound to MANT-ATP since a 10-fold molar excess of CaM relative to EF did not yield a larger FRET with MANT-CTP. The models shown in Fig. 4 suggest a similar binding mode of MANT-CTP and its ATP analog. However, subtle differences due to the nucleobases occur and may account for the higher potency and the small FRET signal of MANT-CTP. In particular, the cytosine moiety may form water-mediated hydrogen bonds with R329 and E580 and favorably fit to the amide dipole of N583. Additionally, the flexibility of the bound cytosine should be greater than in the case of the bulkier adenine ring. Together with the specific charge distribution in the vicinity of the nucleobase, this may lead to absorption and thus attenuation of the FRET energy which is mainly due to tyrosine and tryptophan residues in switch C.

H577 plays a crucial role in catalysis as is reflected by the very low catalytic activity of the H577A mutant (Table 1) (Drum et al., 2002; Guo et al., 2004). Nonetheless, the catalytic activity of the H577A mutant was sufficiently large to

determine substrate- and MANT-nucleotide affinity. Indeed, this mutation does not exert detrimental effect on substrate- and inhibitor binding per se (Tables 1 and 2).

N583 forms a crucial hydrogen bond with the ribosyl moiety of nucleotides bound to the catalytic site of EF (Drum et al., 2002). Accordingly, replacement of N583 by a non-hydrogen bond-forming amino acid (N583A) or hydrogen bond-forming amino acid with a different spatial arrangement of the bonding partners (N583Q and N383H) substantially decreases catalytic activity of the resulting EF mutants and also increases K_m (Table 1) (Drum et al., 2002). Thus, it was also not surprising that N583 mutants substantially reduced the potencies of MANT-ATP and MANT-CTP (Table 2). However, whereas the N583A mutation and the N583H mutation affected inhibitor potencies to a similar extent, the potency of MANT-CTP was much more strongly reduced by the N583Q mutation than the potency of MANT-ATP. These findings suggest that the binding of MANT-CTP is severely impaired by the longer side chain of Q as compared to N, indicative for a substantial spatial constraint in this part of the binding pocket.

The carboxyl group of E588 and the amino group of K353 form an ionic bond that locks the base into the catalytic site (Drum et al., 2002). Disruption of this ionic bond by the K353A mutation largely reduces catalytic activity and lowers substrate affinity (Drum et al., 2002) (Table 1). The K353R mutation that alters the spatial arrangement of the catalytic site but still allows ionic bridge formation displays less severe impairment of catalysis and no change in K_m (Table 1). Intriguingly, binding of MANT-CTP to the catalytic site is much more sensitive to disruption of ionic bond formation between E588 and K353 and reorientation of the ionic bond than binding of MANT-ATP (Table 2), further corroborating the notion that there are subtle differences in the binding modes of MANT-ATP and MANT-CTP.

Molecular Pharmacology Fast Forward. Published on December 4, 2008 as DOI: 10.1124/mol.108.052340
This article has not been copyedited and formatted. The final version may differ from this version.

The high sensitivity of our AC assay, largely due to very low blank values (see Materials and Methods) allowed us not only to precisely determine the kinetic parameters of EF mutants but also of wild-type EF in the absence of CaM. In fact, the catalytic activity of EF is not absolutely CaM-dependent. Even in the absence of CaM, we could accurately determine kinetic parameters using appropriate experimental conditions, i.e. higher protein and [α-^{32}P]ATP amounts, higher incubation temperature and longer incubation time. The fact that in the absence of CaM, EF displays unaltered substrate- and inhibitor affinity despite the largely reduced catalytic activity was rather surprising. Even the MANT-CTP/MANT-ATP potency ratio is conserved. Comparing the crystal structures of EF-CaM (PDB 1lvc, Shen et al., 2002) and EF alone (PDB 1k8t, Drum et al., 2002), 13 mutually resolved amino acids of the MANT-nucleotide binding sites (Fig. 4B) fit very well (RMSD of the backbone atoms 0.99 Å, only G578 and T579 at the N-terminus of switch B are outliers with distances of greater than 1.5 Å). However, switch B stabilized by switch C in EF-CaM is disordered in the structure of EF alone and contains amino acids involved in substrate- and MANT-nucleotide binding to EF-CaM (T579, E580, N583, F586, E588) or in the stabilization of residues that participate in catalysis (e.g., D590 forming a salt bridge with R329). To explain the unaltered potency of the MANT inhibitors at EF alone, we postulate that the nucleotides stabilize switch B in a conformation like that in EF-CaM. The substrate may act similarly in terms of affinity, but the resulting switch B conformation is insufficient for high catalytic activity. Experiments with membrane-permeable CaM inhibitors (Wolberg and Zimmerman, 1984) will have to answer the question whther the CaM-independent catalytic activity of EF is of pathophysiological relevance.

In conclusion, through a combination of enzymological, fluorescence spectroscopy, mutagenesis and molecular modeling approaches, we have shown

Molecular Pharmacology Fast Forward. Published on December 4, 2008 as DOI: 10.1124/mol.108.052340
This article has not been copyedited and formatted. The final version may differ from this version.

that there are subtle differences in the binding modes of MANT-ATP and MANT-CTP to EF. EF, unlike all other ACs studied so far including mAC and CyaA toxin from *Bordetella pertussis*, exhibits a unique preference for the base cytosine, offering an excellent starting point for the development of EF inhibitors with specificity for the toxin relative to mAC. Finally, our studies also raise the intriguing question whether CTP, exhibiting an unusually high affinity for EF is not only an inhibitor of cAMP synthesis but, perhaps, a substrate itself.

Acknowledgment

We thank Mrs. Astrid Seefeld for expert technical assistance. Thanks are also due to the Reviewers of the paper for their helpful critique and suggestions.

Molecular Pharmacology Fast Forward. Published on December 4, 2008 as DOI: 10.1124/mol.108.052340
This article has not been copyedited and formatted. The final version may differ from this version.

References

Ahuja N, Kumar P and Bhatnagar R (2004) The adenylate cyclase toxins. *Crit Rev Microbiol* **30**: 187-196.

Boyd AP, Ross PJ, Conroy H, Mahon N, Lavelle EC and Mills KH (2005) *Bordetella pertussis* adenylate cyclase toxin modulates innate and adaptive immune responses: distinct roles for acylation and enzymatic activity in immunomodulation and cell death. *J Immunol* **175**: 730-738.

Carbonetti NH, Artamonova GV, Andreasen C and Bushar N (2005) *Pertussis* toxin and adenylate cyclase toxin provide a one-two punch for establishment of *Bordetella pertussis* infection of the respiratory tract. *Infect Immun* **73** :2698-2703.

Clark M, Cramer R.D. III and Van Opdenbosch N (1989) Validation of the general purpose Tripos 5.2 force field. *J Comp Chem* **10**:982-1012.

Confer DL and Eaton JW (1982) Phagocyte impotence caused by an invasive bacterial adenylate cyclase. *Science* **217**: 948-950.

Cornell WD, Cieplak P, Bayly CI, Gould IR, Merz KMJ, Ferguson DM, Spellmeyer DC, Fox T, Caldwell JW and Kollman PA (1995) A second generation force field for the simulation of proteins and nucleic acids. *J Am Chem* **117**:5179-5197.

Drum CL, Yan SZ, Bard J, Shen YQ, Lu D, Soelaiman S, Grabarek Z, Bohm A and Tang WJ (2002) Structural basis for the activation of anthrax adenylyl cyclase exotoxin by calmodulin. *Nature (London)* **415**: 396-402.

Gille A, Lushington GH, Mou TC, Doughty MB, Johnson RA and Seifert R (2004) Differential inhibition of adenylyl cyclase isoforms and soluble guanylyl cyclase by purine and pyrimidine nucleotides. *J Biol Chem* **279**: 19955-19969.

Gille A, Guo J, Mou TC, Doughty MB, Lushington GH and Seifert R (2005) Differential interactions of G-proteins and adenylyl cyclase with nucleoside 5'-triphosphates, nucleoside 5'-[γ-thio]phosphates and nucleoside 5'-[β,γ-imido]triphosphates. *Biochem Pharmacol* **71**: 89-97.

Gille A and Seifert R (2003) 2'(3')-*O*-(*N*-methylanthraniloyl)-substituted GTP analogs: a novel class of potent competitive adenylyl cyclase inhibitors. *J Biol Chem* **278**: 12672-12679.

Gilles AM, Munier H, Rose T, Glaser P, Krin E, Danchin A, Pellecuer C and Barzu O (1990) Intrinsic fluorescence of a truncated *Bordetella pertussis* adenylate cyclase expressed in *Escherichia coli*. *Biochemistry* **29**: 8126-8130.

Göttle M, Dove S, Steindel P, Shen Y, Tang W-J, Geduhn J, König B, Seifert R (2007) Molecular analysis of the interaction of *Bordetella pertussis* adenylyl cyclase with fluorescent nucleotides. *Mol. Pharmacol.* **72**: 526-535.

Gopalakrishna R and Anderson WB (1982) Ca^{2+}-induced hydrophobic site on calmodulin: Application for purification of calmodulin by phenyl-Sepharose affinity chromatography. *Biochem Biophys Res Commun* **104**: 830-836.

Guo Q, Shen Y, Zhukovskaya NL, Florian J and Tang WJ (2004) Structural and kinetic analyses of the interaction of anthrax adenylyl cyclase toxin with reaction products cAMP and pyrophosphate. *J Biol Chem* **279**: 29427-29435.

Guo Q, Shen Y, Lee YS, Gibbs CS, Mrksich M and Tang WJ (2005) Structural basis for the interaction of *Bordetella pertussis* adenylyl cyclase toxin with calmodulin. *EMBO J* **24**: 3190-3201.

Hewlett EL, Donato GM and Gray MC (2006) Macrophage cytotoxicity produced by adenylate cyclase toxin from *Bordetella pertussis*: more than just making cyclic AMP! *Mol Microbiol* **59**: 447-459.

Hewlett EL, Gordon VM, McCaffery JD, Sutherland WM and Gray MC (1989) Adenylate cyclase toxin from *Bordetella pertussis*. Identification and purification of the holotoxin molecule. *J Biol Chem* **264**: 19379-19384.

Hiratsuka T (1983) New ribose-modified fluorescent analogs of adenine and guanine nucleotides available as substrates for various enzymes. *Biochim Biophys Acta* **742**: 496-508.

Hiratsuka T (2003) Fluorescent and colored trinitrophenylated analogs of ATP and GTP. *Eur J Biochem* **270**: 3479-3485.

Hong J, Beeler J, Zhukovskaya NL, He W, Tang WJ, Rosner MR (2005) Anthrax edema factor potency depends on mode of cell entry. *Biochem. Biophys. Res. Commun.* **335**: 850-857.

Jameson DM and Eccleston JF (1997) Fluorescent nucleotide analogs: synthesis and applications. *Methods Enzymol* **278**: 363-390.

Jedrzejas MJ (2002) The structure and function of novel proteins of *Bacillus anthracis* and other spore-forming bacteria: development of novel prophylactic and therapeutic agents. *Crit. Rev. Biochem. Mol. Biol.* **37**: 339-373.

Johnson RA and Shoshani I (1990) Inhibition of *Bordetella pertussis* and *Bacillus anthracis* adenylyl cyclases by polyadenylate and "P"-site agonists. *J Biol Chem* **265**: 19035-19039.

Ladant D and Ullmann A (1999) *Bordatella pertussis* adenylate cyclase: a toxin with multiple talents. *Trends Microbiol* **7**: 172-176.

Lakowicz JR (1999) *Principles of fluorescence spectroscopy*. Kluwer Academic/Plenum, New York.

Mock M and Ullmann A (1993) Calmodulin-activated bacterial adenylate cyclases as virulence factors. *Trends Microbiol* **1**: 187-192.

Moreland JL, Gramada A, Buzko OV, Zhang Q and Bourne PE (2005) The Molecular Biology Toolkit (MBT): a modular platform for developing molecular visualization applications. *BMC Bioinformatics* **6**: 21.

Mou TC, Gille A, Fancy DA, Seifert R and Sprang SR (2005) Structural basis for the inhibition of mammalian membrane adenylyl cyclase by 2 '(3')-*O*-(*N*-methylanthraniloyl)-guanosine 5'-triphosphate. *J Biol Chem* **280**: 7253-7261.

Mou TC, Gille A, Suryanarayana S, Richter M, Seifert R and Sprang SR (2006) Broad specificity of mammalian adenylyl cyclase for interaction with 2',3'-substituted purine- and pyrimidine nucleotide inhibitors. *Mol Pharmacol* **70**: 878-886.

Sarfati RS, Kansal VK, Munier H, Glaser P, Gilles AM, Labruyere E, Mock M, Danchin A and Barzu O (1990) Binding of 3'-anthraniloyl-2'-deoxy-ATP to calmodulin-activated adenylate cyclase from *Bordetella pertussis* and *Bacillus anthracis*. *J Biol Chem* **265**: 18902-18906.

Shen Y, Lee YS, Soelaiman S, Bergson P, Lu D, Chen A, Beckingham K, Grabarek Z, Mrksich M and Tang WJ (2002) Physiological calcium concentrations regulate calmodulin binding and catalysis of adenylyl cyclase exotoxins. *EMBO J* **21**: 6721-6732.

Shen Y, Zhukovskaya NL, Zimmer MI, Soelaiman S, Bergson P, Wang CR, Gibbs CS and Tang WJ (2004) Selective inhibition of anthrax edema factor by adefovir, a drug for chronic hepatitis B virus infection. *Proc Natl Acad Sci USA* **101**: 3242-3247.

Shen Y, Zhukovskaya NL, Guo Q, Florián J, Tang WJ (2005) Calcuim-independent calmodulin binding and two-metal-ion catalytic mechanism of anthrax edema factor. *EMBO J.* **24**: 929-941.

Soelaiman S, Wei BQ, Bergson P, Lee YS, Shen Y, Mrksich M, Shoichet BK and Tang WJ (2003) Structure-based inhibitor discovery against adenylyl cyclase toxins from pathogenic bacteria that cause anthrax and whooping cough. *J Biol Chem* **278**: 25990-25997.

Wang JL, Guo JX, Zhang QY, Wu JJ, Seifert R, Lushington GH (2007) A conformational transition in the adenylyl cyclase catalytic site yields different binding modes for ribosyl-modified and unmodified nucleotide inhibitors. *Bioorg. Med. Chem.* **15**: 2993-3002.

Wolberg G, Zimmerman TP (1984) Effects of calmodulin antagonists on immune mouse lymphocytes. *Mol Pharmacol* **26**: 286-292.

Molecular Pharmacology Fast Forward. Published on December 4, 2008 as DOI: 10.1124/mol.108.052340
This article has not been copyedited and formatted. The final version may differ from this version.

Footnotes

[†]Supported by the Deutsche Forschungsgemeinschaft (Graduiertenkolleg 760 "Medicinal Chemistry: Molecular Recognition - Ligand-Receptor Interactions" and research grant Se 529/5-1 to R.S.). H.M.T. is supported by a predoctoral fellowship of the Arabic Republic of Egypt. J.S. was supported by the “International Study and Training Partnerships (ISAP) Program” of the German Academic Exchange Service (DAAD).

[1]present address: Department of Pathology, School of Medicine, University of Regensburg, Germany

[2]present address: Research & Development, Cardiovascular Diseases, Sanofi-Aventis, Frankfurt/Main, Germany

[3]Send reprint requests to:
Dr. Roland Seifert
Department of Pharmacology,
Medical School of Hannover
Carl-Neuberg-Straße 1
D-30625 Hannover, Germany
Telephone: +49-511-532-2805. Fax: +49-511-532-4081.
E-mail: seifert.roland@mh-hannover.de

Molecular Pharmacology Fast Forward. Published on December 4, 2008 as DOI: 10.1124/mol.108.052340
This article has not been copyedited and formatted. The final version may differ from this version.

Figure legends

Figure 1. Lineweaver-Burk analysis of the inhibition of EF3 AC activity by MANT-ATP and MANT-CTP. AC activities were determined as described under "Materials and Methods" with the indicated concentrations of MANT-ATP (0 μM, 0.5 μM, 5 μM, 10 μM and 20 μM) (**A**) and MANT-CTP (0 μM, 0.5 μM, 1 μM and 5 μM) (**B**). Reaction mixtures contained 10 pM EF3, 100 mM KCl, 100 μM free Ca^{2+}, 5 mM free Mn^{2+}, 100 μM EGTA, 100 μM cAMP, 100 nM calmodulin, 0.2 μCi/tube [α–^{32}P]ATP and unlabeled ATP/Mn^{2+} concentrations indicated in the graph. Data were plotted reciprocally and analyzed by linear regression according to Lineweaver-Burk. Shown are the results of a representative experiment performed in triplicates. Similar results were obtained in two independent experiments.

Figure 2. Analysis of MANT-nucleotide binding to the catalytic site of EF3 and EF3(F586A) using FRET. FRET experiments were performed as described under "Materials and Methods". The assay buffer consisted of 75 mM HEPES/NaOH, 100 μM $CaCl_2$, 100 mM KCl and 5 mM $MnCl_2$, pH 7.4. Nucleotides were added to the buffer to yield 300 nM final concentrations. EF3/EF3(F586A) (300 nM final concentration) was added followed by the addition of CaM (1 μM final concentration). Emission was scanned at an excitation wavelength of 280 nm after each addition. The buffer and the MANT-nucleotide basal fluorescence was subtracted from the fluorescence after addition of EF3/EF3(F586A) (dotted purple line) and CaM (solid blue line). Shown are superimposed recordings of a representative experiment. Similar data were obtained in 5 independent experiments. a.u., arbitrary unit.

Molecular Pharmacology Fast Forward. Published on December 4, 2008 as DOI: 10.1124/mol.108.052340
This article has not been copyedited and formatted. The final version may differ from this version.

Figure 3. Kinetic analysis of the interaction of EF3 with MANT-nucleotides and CaM in FRET experiments. Kinetic experiments were performed as described in "Materials and Methods". The excitation wavelength was 280 nm and emission was detected at 430 nm over time. Successively, buffer (**1**), 300 nM EF3 (**2**), 1 µM CaM (**3**), nucleotide (**A**: MANT-ATP, **B**: MANT-CTP, 300 nM each) (**4**) and PMEApp (1 µM) (**5**) were added. A recording of a representative experiment is shown. Similar data were obtained in 4 independent experiments. a.u., arbitrary unit.

Figure 4. Docking of MANT- CTP and MANT-ATP on EF-CaM. The minimized models are based on the crystal structure of EF-CaM-3'ANT-2'deoxy-ATP, PDB 1lvt (Shen et al., 2002). Colors of atoms, unless otherwise indicated: P – orange, O – red, N – blue, C, H –grey, Mg^{2+} – purple spheres. **A**, topology diagram of the EF domains surrounding the binding site with docked 3'-MANT-CTP (represented as transparent CPK model). Domains C_A – green, C_B – greenblue, switch A – red, switch B – orange, switch C – yellow. Amino acids subjected to mutation – balls and sticks models. **B-D**, detailed representation of interactions of MANT-nucleotides with EF-CaM. The side chains of amino acids within a sphere of 3 Å around the ligand and Mg^{2+} are drawn as sticks (C atoms – cyan) and labeled. For clarity, repeating labels are omitted in panels C and D (see panel B). Cα-trace – cyan line. **B**, docking of 3´-MANT-CTP. **C**, docking of 2´-MANT-CTP. **D**, docking of 3´-MANT-ATP. **E**, superposition of the docked MANT nucleotides based on alignment of the three EF models (all heavy protein atoms considered). Colors of C and essential H atoms: 3´-MANT-CTP – green, 2´-MANT-CTP – purple, 3´-MANT-ATP – yellow.

Molecular Pharmacology Fast Forward. Published on December 4, 2008 as DOI: 10.1124/mol.108.052340
This article has not been copyedited and formatted. The final version may differ from this version.

Table 1. K_m and V_{max} values of EF, EF3 and various EF3 mutants

Toxin	Ca^{2+}/CaM	V_{max} (s^{-1})	K_m (μM)
EF	+	232 ± 34	84.5 ± 8.3
EF3	+	223 ± 12	82.6 ± 8.2
EF3(F586A)	+	128 ± 5.0	92.0 ± 14.7
EF3(H577A)	+	0.013 ± 0.003	34.5 ± 9.7
EF3(N583A)	+	15.4 ± 0.13	224 ± 7.3
EF3(N583Q)	+	18.4 ± 0.08	855 ± 39
EF3(N583H)	+	59.7 ± 10.4	3,890 ± 1,220
EF3(K353A)	+	3.93 ± 0.02	804 ± 137
EF3(K353R)	+	32.3 ± 0.06	75.4 ± 1.35
EF3	-	0.11 ± 0.007	60.0 ± 0.89

AC toxin activities were determined as described under "Materials and Methods". K_m and V_{max} values were obtained by non-linear regression analysis of substrate-saturation experiments and are the means ± SD of at least 3 independent experiments performed in triplicates. For the determination of the V_{max} and K_m of EF, EF3 and EF3(F586A), reaction mixtures contained100 μM free Ca^{2+}, 5 mM free Mn^{2+}, 100 μM EGTA, 0.2-1.0 μCi/tube [α–^{32}P]ATP, 100 μM cAMP, 100 nM calmodulin and 10 pM enzyme in 75 mM Tris/HCl, pH 7.4. In case of the other EF3 mutants, reaction mixtures contained 0.4 μCi [α–^{32}P]ATP per tube and 2 nM enzyme. For determination of V_{max} and K_m without CaM and Ca^{2+}, the enzyme concentration was 5 nM. The unlabeled ATP/Mn^{2+} concentrations ranged from 100 nM to 4 mM as appropriate to obtain saturated curves.

Molecular Pharmacology Fast Forward. Published on December 4, 2008 as DOI: 10.1124/mol.108.052340
This article has not been copyedited and formatted. The final version may differ from this version.

Table 2. Inhibitory potencies of MANT-ATP and MANT-CTP at EF, EF3 and EF3 mutants in the presence of Mn^{2+}

Toxin	Ca^{2+}/CaM	MANT-ATP K_i (μM)	MANT-ATP rel. pot.	MANT-CTP K_i (μM)	MANT-CTP rel. pot.
EF	+	0.58 ± 0.13	169	0.11 ± 0.04	91
EF3	+	0.98 ± 0.08	100	0.10 ± 0.008	100
E3(F586A)	+	4.54 ± 1.15	22	0.61 ± 0.11	16
EF3(H577A)	+	0.52 ± 0.05	189	0.11 ± 0.017	91
EF3(N583A)	+	91.7 ± 2.5	1.1	10.4 ± 0.02	1.0
EF3(N583Q)	+	67.4 ± 4.8	1.5	248 ± 23	0.04
EF3(N583H)	+	308 ± 89	0.3	22 ± 5.4	0.5
EF3(K353A)	+	17.4 ± 4.0	5.6	54.8 ± 0.83	0.2
EF3(K353R)	+	3.27 ± 0.08	30	6.53 ± 0.26	1.5
EF3	-	1.07 ± 0.04	92	0.16 ± 0.02	63

Inhibitory potencies of MANT-ATP and MANT-CTP at EF, EF3 and various EF3 mutants were determined as described under "Materials and Methods". K_i-values are given in μM and are the means ± SD of 3 experiments performed in triplicates. The relative potencies (rel. pot.) of MANT-ATP and MANT-CTP are given, too, EF3 being the reference. For determination of the inhibitory potencies of MANT-ATP and MANT-CTP at EF, EF3 and EF3(F586A), reaction mixtures contained100 μM free Ca^{2+}, 5 mM free Mn^{2+}, 100 μM EGTA, 40 μM ATP, 0.2-1.0 μCi/tube [α–^{32}P]ATP, 100 μM cAMP, 100 nM CaM and10 pM enzyme in 75 mM Tris/HCl, pH 7.4. For other EF3 mutants, reaction mixtures contained 1.0 μCi [α–^{32}P]ATP per tube. The enzyme concentration was 2 nM. For the determination of K_i-values of MANT-ATP and MANT-CTP without CaM and Ca^{2+}, the ATP/Mn^{2+} concentration was 20 μM and the enzyme concentration was 5 nM. Nucleotides were added at different concentrations as appropriate to obtain saturated concentration-response curves. Inhibition curves were analyzed by non-linear regression using the Prism 4.02 software.

Molecular Pharmacology Fast Forward. Published on December 4, 2008 as DOI: 10.1124/mol.108.052340
This article has not been copyedited and formatted. The final version may differ from this version.

Table 3: Inhibitory potencies of NTPs and (M)ANT-nucleotides at EF in the presence of Mn^{2+} and Mg^{2+}

Nucleotide	K_i (μM)	
	Mn^{2+}	Mg^{2+}
GTP	9.2 ± 0.79	73.6 ± 6.02
ITP	45.4 ± 3.60	233 ± 15.8
UTP	63.9 ± 9.21	138 ± 2.53
CTP	5.10 ± 0.38	45.2 ± 9.18
MANT-ATP	0.58 ± 0.09	1.36 ± 0.57
MANT-ADP	3.26 ± 0.50	34.7 ± 3.34
ANT-ATP	0.44 ± 0.09	5.15 ± 2.12
ANT-ADP	3.85 ± 1.25	57.9 ± 25.1
MANT-GTP	2.49 ± 0.08	4.70 ± 0.32
ANT-GTP	4.10 ± 1.09	13.0 ± 1.86
MANT-ITP	4.06 ± 0.06	10.6 ± 3.29
MANT-IDP	11.0 ± 1.89	48.5 ± 3.16
MANT-UTP	3.67 ± 0.08	32.2 ± 0.82
MANT-UDP	38.7 ± 0.48	107 ± 20.6
MANT-CTP	0.10 ± 0.01	1.26 ± 0.09
MANT-CDP	1.30 ± 0.12	13.8 ± 0.06

Inhibitory potencies of various purine and pyrimidine nucleotides at EF were determined as described under "Materials and Methods". K_i values are given in μM and are the means ± SD of 3-4 independent experiments performed in triplicates. The K_m value of EF for ATP in the presence of Mg^{2+} was 120 ± 6.5 μM. Reaction mixtures contained 5 mM $MnCl_2$ or 5 mM $MgCl_2$, 100 mM KCl, 100 μM $CaCl_2$, 40 μM ATP, [α–^{32}P]ATP (0.2-0.4 μCi/tube), 100 μM cAMP and 100 nM CaM. Nucleotides were added at different concentrations as appropriate to construct saturated concentration-response curves. Inhibition curves were analyzed by non-linear regression using the Prism 4.02 software.

Molecular Pharmacology Fast Forward. Published on December 4, 2008 as DOI: 10.1124/mol.108.05
This article has not been copyedited and formatted. The final version may differ from this versio

Figure 1

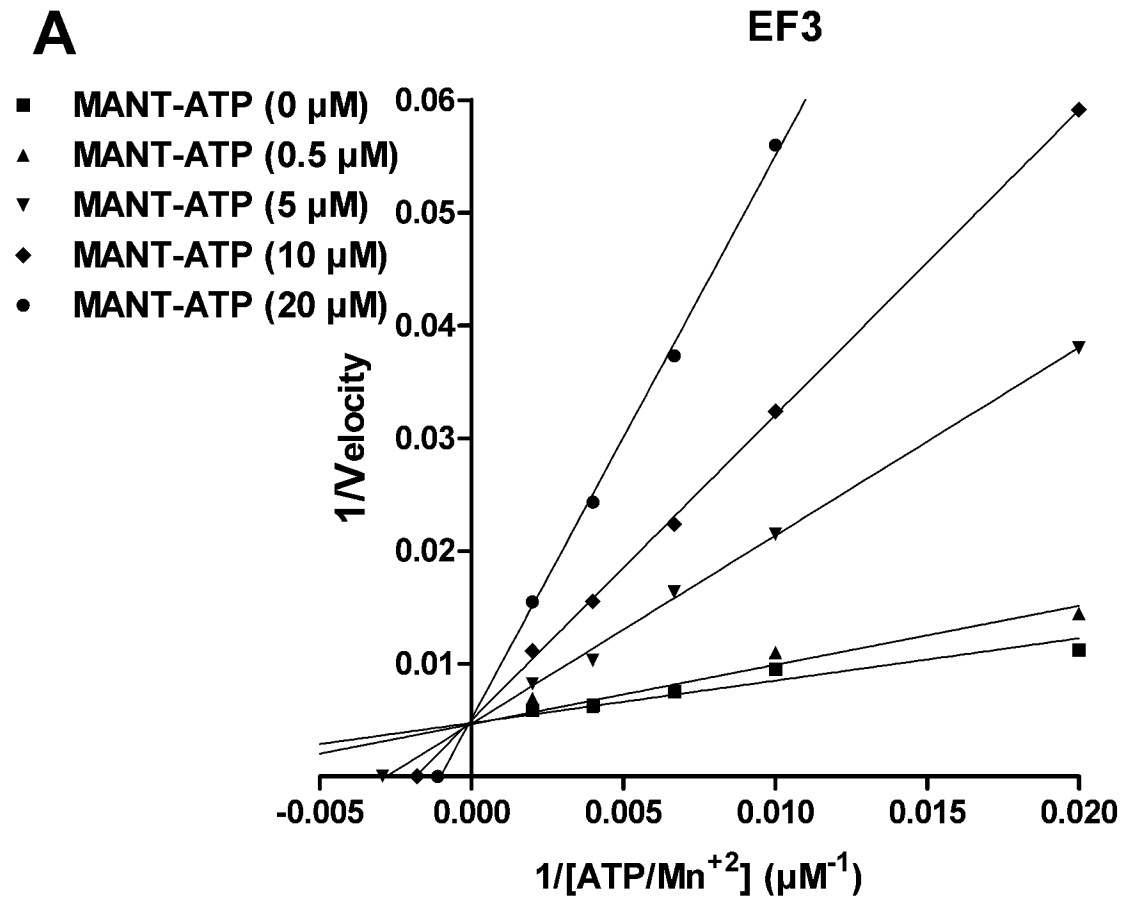

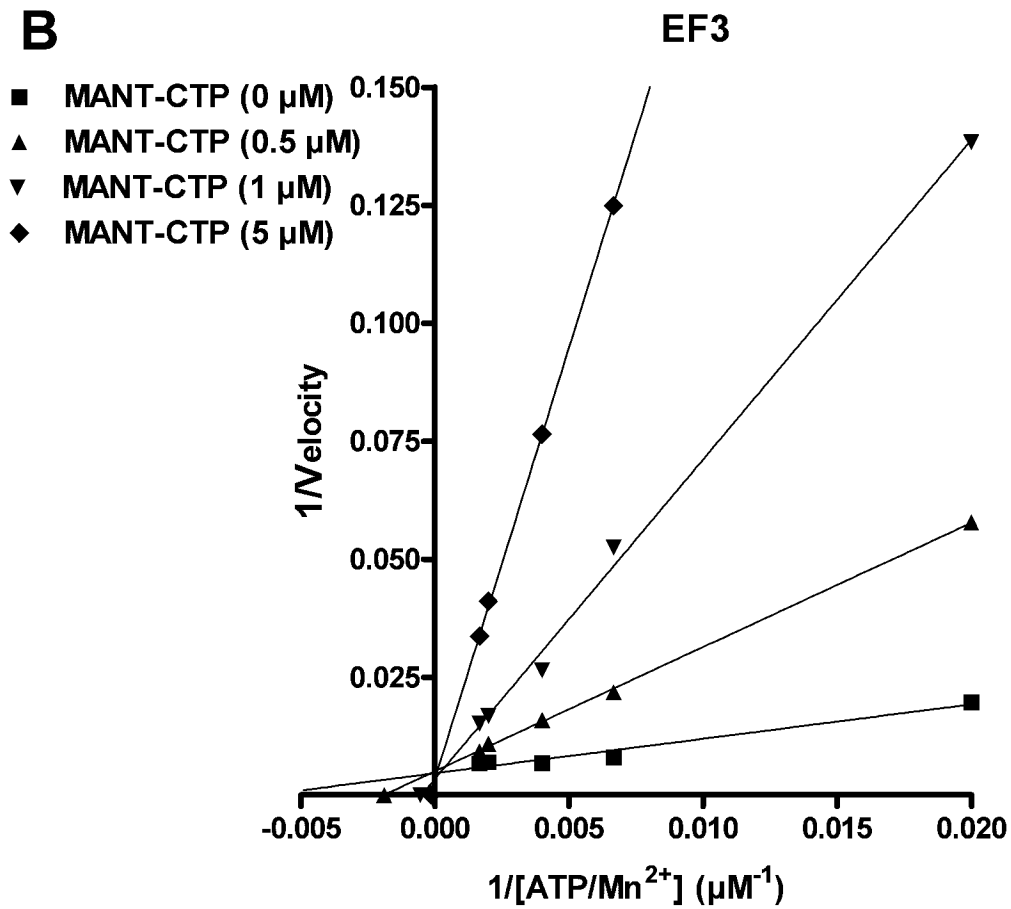

Figure 2

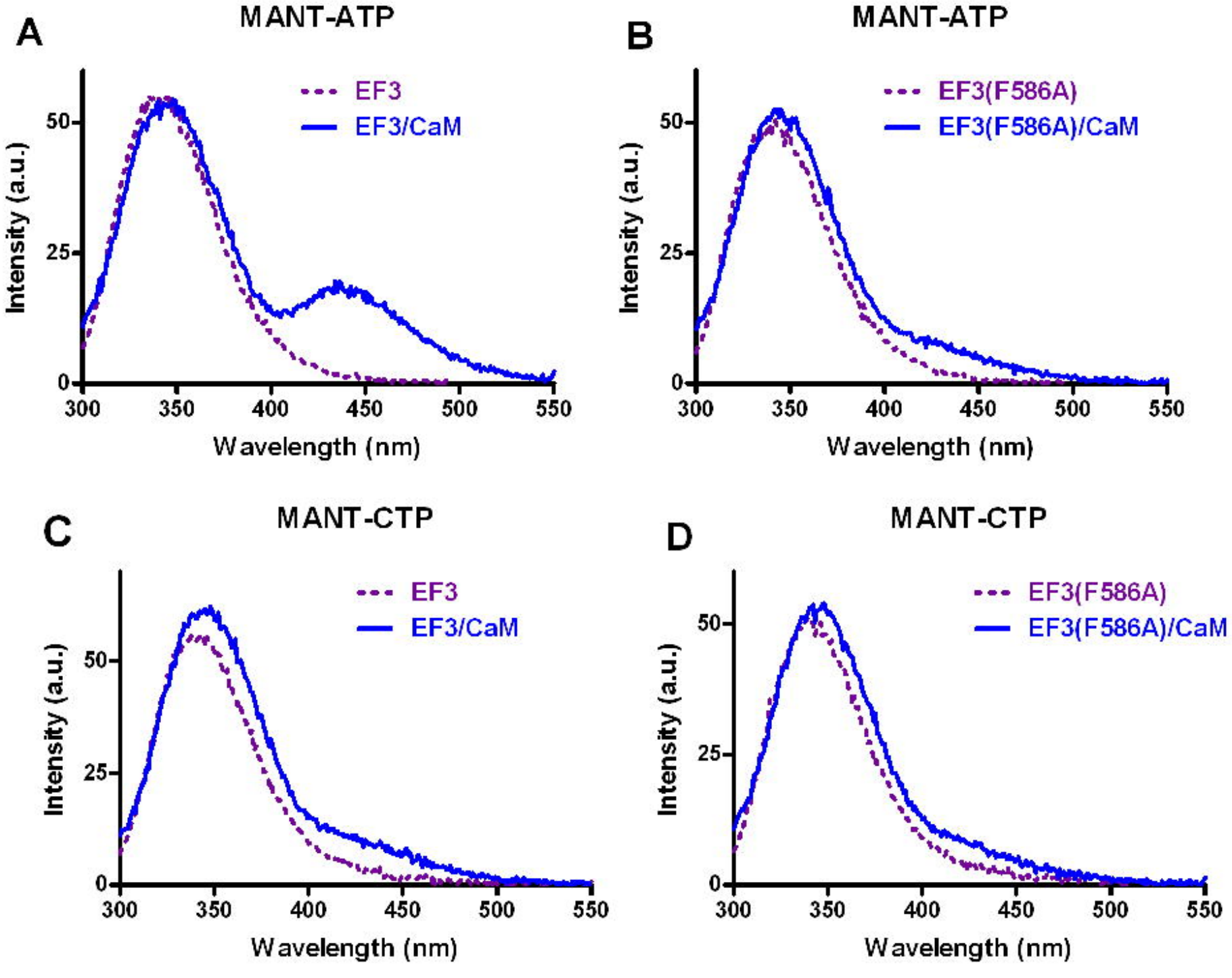
A
MANT-ATP
EF3
EF3/CaM
Intensity (a.u.)
0
25
50
300
350
400
450
500
550
Wavelength (nm)
B
MANT-ATP
EF3(F586A)
EF3(F586A)/CaM
Intensity (a.u.)
0
25
50
300
350
400
450
500
550
Wavelength (nm)
C
MANT-CTP
EF3
EF3/CaM
Intensity (a.u.)
0
25
50
300
350
400
450
500
550
Wavelength (nm)
D
MANT-CTP
EF3(F586A)
EF3(F586A)/CaM
Intensity (a.u.)
0
25
50
300
350
400
450
500
550
Wavelength (nm)

Figure 3

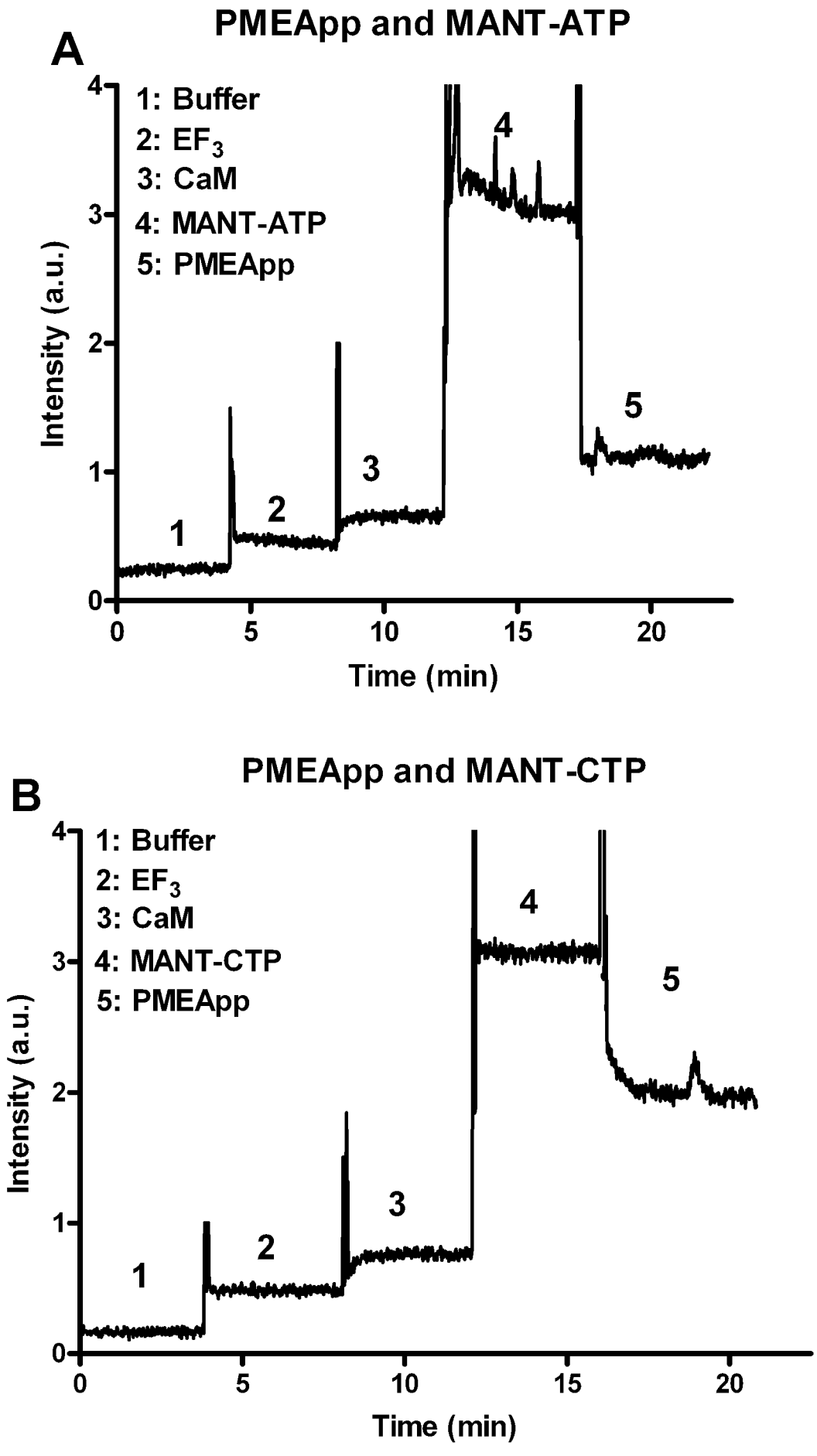

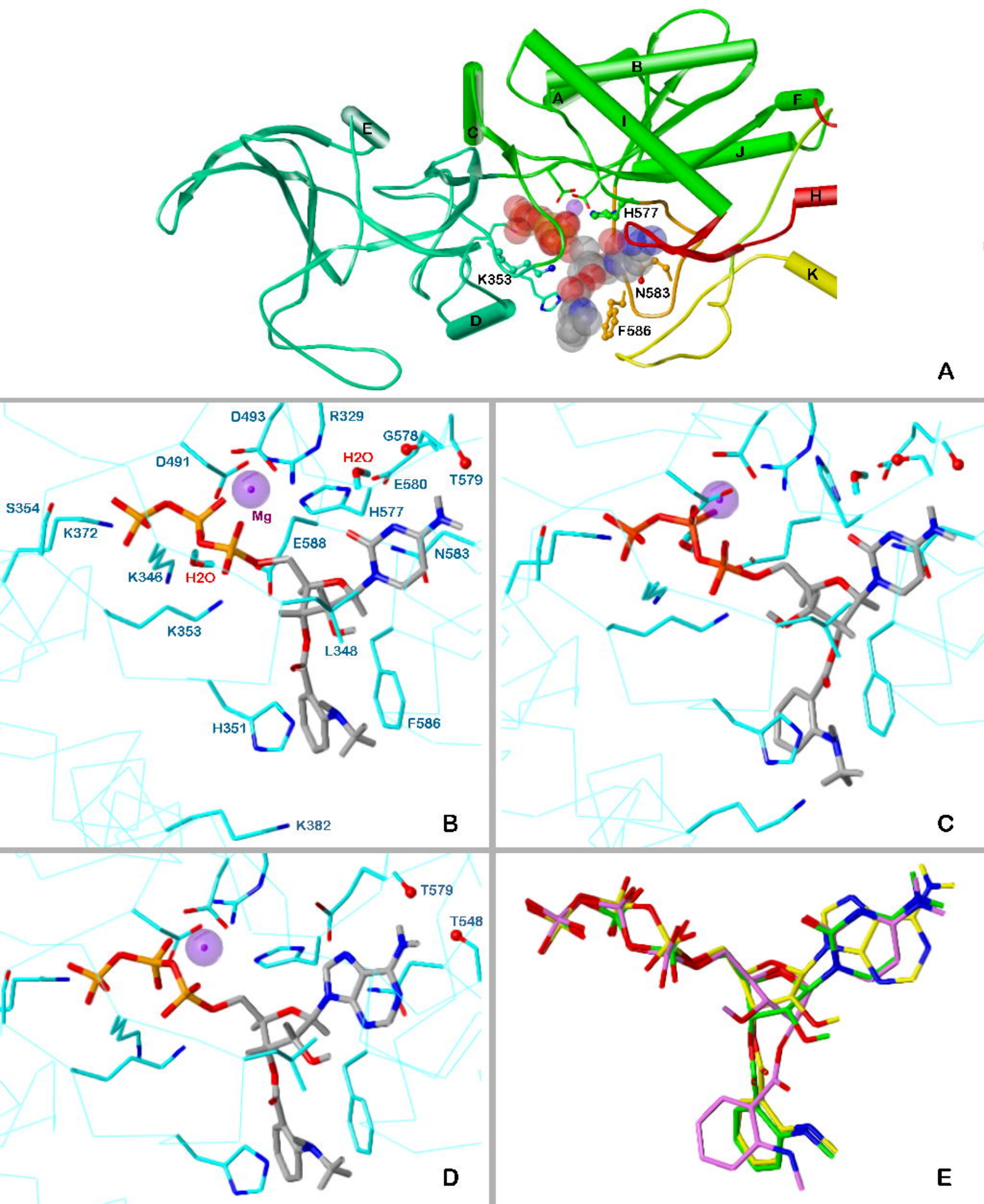
B
A
F
I
J
H
E
C
H577
K
K353
N583
D
F586
A
D493
R329
G578
D491
H2O
T579
E580
S354
Mg
H577
K372
E588
N583
K346
H2O
K353
L348
H351
F586
K382
B
C
T579
T548
D
E